Biomed Microdevices (2017) 19: 46
DOI 10.1007/s10544-017-0189-9

Accelerated life-test methods and results for implantable electronic devices with adhesive encapsulation

Xuechen Huang[1,2] · **Petcharat May Denprasert**[2] · **Li Zhou**[1] · **Adriana Nicholson Vest**[1] · **Sam Kohan**[2] · **Gerald E. Loeb**[1,2]

Published online: 24 May 2017
© Springer Science+Business Media New York 2017

Abstract We have developed and applied new methods to estimate the functional life of miniature, implantable, wireless electronic devices that rely on non-hermetic, adhesive encapsulants such as epoxy. A comb pattern board with a high density of interdigitated electrodes (IDE) could be used to detect incipient failure from water vapor condensation. Inductive coupling of an RF magnetic field was used to provide DC bias and to detect deterioration of an encapsulated comb pattern. Diodes in the implant converted part of the received energy into DC bias on the comb pattern. The capacitance of the comb pattern forms a resonant circuit with the inductor by which the implant receives power. Any moisture affects both the resonant frequency and the Q-factor of the resonance of the circuitry, which was detected wirelessly by its effects on the coupling between two orthogonal RF coils placed around the device. Various defects were introduced into the comb pattern devices to demonstrate sensitivity to failures and to correlate these signals with visual inspection of failures. Optimized encapsulation procedures were validated in accelerated life tests of both comb patterns and a functional neuromuscular stimulator under development. Strong adhesive bonding between epoxy and electronic circuitry proved to be necessary and sufficient to predict 1 year packaging reliability of 99.97% for the neuromuscular stimulator.

Keywords Accelerated life test · Non-hermetic packaging · Encapsulation · Wireless · Implantable

✉ Xuechen Huang
xuechenh@usc.edu

[1] Department of Biomedical Engineering, University of Southern California, Los Angeles, CA, USA

[2] General Stim Inc., Los Angeles, CA, USA

1 Introduction

A long functional lifetime is critical for clinical applications of most implantable medical devices. This is usually evaluated by accelerated life-testing in which failure modes that might occur after years of normal use are revealed more quickly by increasing the temperature and duty cycle. One common source of failures is the device packaging that is designed to protect the electronic components from body fluids and protects the body from the electronic components (Stieglitz 2010). Hermetic packages employing exotic metal and ceramic technologies have few long-term failure modes but tend to result in relatively expensive, bulky and rigid devices that must be implanted surgically. For applications requiring treatment for months to years rather than decades, such packaging is unnecessary. Polymeric encapsulation was used with considerable success in the early days of pacemakers and spinal cord stimulators. Non-hermetic encapsulated devices can be inexpensive and reliable, permitting small and elongated shapes that can be implanted via minimally invasive procedures (Kim et al. 2009, Stieglitz 2010). However, this type of encapsulation may still fail within months to years due to diffusion and condensation of water vapor and corrosion of electronic components (Hassler et al. 2011, Wang et al. 2013). Its integrity depends on conformal layer adhesion to component surfaces rather than a diffusion barrier (Vanhoestenberghe and Donaldson 2013). Such adhesion can fail over time as a result of various stressors, so it is important to test such devices under actual use conditions, but it may be impractical to do so for the design life of the device. The alternative is to introduce higher than usual aging factors (such as temperature, voltage, pressure, usage level, etc., or combinations thereof) to cause test units to fail more rapidly than under usual conditions (Nelson 1980, Escobar and Meeker

2006). It is also important, however, to avoid introducing failure modes that may be specific to the test methods, such as adding connections to energizing and monitoring instrumentation.

The most commonly used acceleration factor is elevated temperature, but many components including the polymeric encapsulant may have limited operating temperature ranges, such as its glass transition temperature. An alternative is to detect incipient failure at an early stage by using a highly sensitive test device. Rather than waiting for water to condense, corrode and cause circuit failure, a more sensitive "comb pattern" consisting of many closely interdigitated elements is used detect initial water molecule diffusion and condensation. Traditionally, the encapsulated comb pattern device is made with two wire connections to an external power source for DC bias voltage and to an impedance spectrometer to monitor package performance (Bierwagen et al. 2003). A DC bias applied across the comb pattern results in a uniformly high voltage stress (V/cm) over a large test area. Moisture between the electrodes of the comb pattern greatly increases the capacitance and reduces the resistance between them. The combination of elevated temperature, elevated voltage stress, and high sensitivity to incipient failure provides an accelerated validation of encapsulants.

Connecting external leads to the comb pattern may be difficult or impossible without changing the structure and fabrication procedure of the clinical device, which can lead to inaccurate extrapolation of lifetime and reliability (Yacobi et al. 2002). Furthermore, lead connection may not even be possible for the next generation of devices that use bi-directional wireless transmission of power and data (Loeb et al. 2001, Zhou et al. 2016). Some implantable devices such as RF identification (RFID) "biochips", video cameras, photonic stimulators and drug delivery pumps may not normally have any externalized electrical connections (Gensler et al. 2012, Koulaouzidis et al. 2015). We utilized non-contact methods to detect changes in the resonance of tuned inductor-capacitor circuits, which have long been used in radio engineering, intracranial pressure monitors (Chubbuck 1977) and other applications (Ong and Grimes 2000).

In this study, we have developed and tested wireless accelerated life-testing methods to evaluate the epoxy packaging performance of a wireless neuromuscular microstimulator called NuStim™, which is designed to exercise the pelvic floor muscle in stress urinary incontinence patients for up to one year (Huang et al. 2017). The ceramic circuit board in the microstimulator was replaced by the comb pattern board to increase sensitivity to incipient failure mechanisms. The devices were stressed by increased temperature, voltage and duty cycle in saline. We developed a non-contact method to measure the resonant frequency and quality factor of the capacitive comb pattern connected to the same inductive coil that normally receives power. Comb pattern devices with different known defects were tracked over time to validate sensitivity to failure mechanisms. Different cleaning and fabrication procedures were compared during the study. Failure rates under these accelerated conditions were extrapolated mathematically to estimate package reliability under normal use conditions for the microstimulator.

2 Design and methods

2.1 Comb pattern

The comb pattern device (Fig. 1a) used the same construction as the microstimulator (Fig. 1b) described elsewhere (Huang et al. 2017). The package consists of a thin-wall borosilicate glass sleeve that was filled with a low permeability epoxy (Epotek #302-3 M, Epoxy Technology Inc.). The comb pattern was printed on an aluminum oxide ceramic substrate (2.4 mm width × 3 mm length) by photolithography (deposited layers of gold over nickel, gold, and titanium-tungsten) with the spacing between the electrodes about 25 μm, as shown in Fig. 2a. The surface mount discrete components were placed on the ceramic PCB board by hotplate soldering at 230 °C (solder paste: WS488-SAC305, AIM solder, CA, USA). The external radio frequency power was received by a machined ferrite core with wound coil (26.5 turns of 0.003″ insulated copper). The complete electronic assembly was cleaned thoroughly as described below and slipped into a clean glass capillary. The epoxy was de-gassed in a vacuum chamber, drawn into a syringe, and centrifuged to further remove bubbles. Then the epoxy was injected through a plastic tube slipped over the subassembly while applying a vacuum to the other end. The epoxy was cured at 40 °C and 230 psi to accelerate polymer crosslinking and prevent dissolved air from forming bubbles. After overnight curing, the plastic tube and excess epoxy was cut away and the electrode surfaces exposed cleanly by abrasive buffing.

The interdigitated electrodes of the comb pattern function as a capacitor C that was connected in parallel with the winding coil L to achieve inductive power transmission and encapsulation failure detection (Fig. 2b). The capacitor C and the inductive coil L in parallel resonate at a frequency f_{SRF}, determined by:

$$f_{SRF} = \frac{1}{2\pi\sqrt{LC}} \tag{1}$$

The value of capacitance C depends on the dielectric properties of the material between the electrodes. Any condensed moisture present will substantially increase C because the dielectric constant of water ($\varepsilon = 80.4$) is much larger than epoxy ($\varepsilon = 3.6$). This will change the self-resonant frequency of the circuit. Condensed moisture will also greatly reduce the resistance between the electrodes of the comb pattern by providing

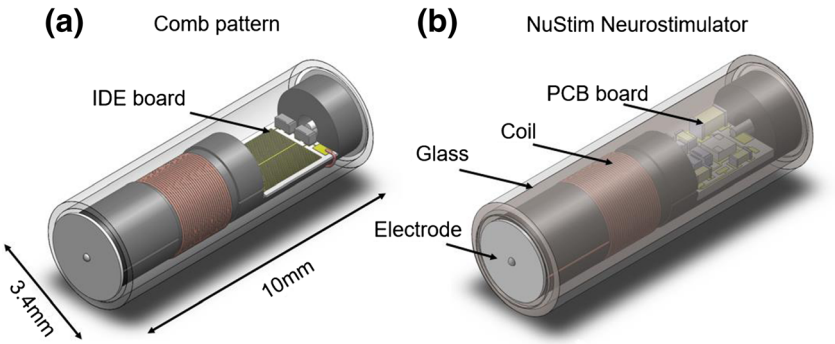

Fig. 1 Design of comb pattern device compared to clinical NuStim microstimulator. **a** Comb pattern device before epoxy filling. **b** Microstimulator after encapsulation

a conductive liquid path between them. This can be detected by a decrease in the quality factor (Q factor) of the circuit based on the equation for a RLC parallel circuit,

$$Q = R\sqrt{\frac{C}{L}} = \frac{f_{SRF}}{\Delta f} \quad (2)$$

The Q factor can be computed by dividing the self-resonant frequency f_{SRF} by the bandwidth Δf, where Δf is identified by a 3db decrease in the amplitude of a received RF signal.

The comb pattern device has the functionality to introduce DC bias voltage as an accelerating stressor. The comb pattern board is separated into two capacitors C1 and C2 in parallel as shown in the schematic (Fig. 2b). The introduced Zener diodes (GDZT2R8.2, Rohm Semiconductor) do not affect the resonant frequency of the circuit, which is mainly determined by the parallel C1 and C2. One side of the comb pattern C1 is connected to the inductive coil terminals directly to receive the AC signal. The other half of the comb pattern C2 is connected in series with the Zener diodes to introduce a DC voltage bias between the capacitor electrodes. A high voltage sinusoidal AC signal is generated across C1 and C2 branches equally during resonance. The Zener diodes provide half-wave rectification that is limited to the reverse-bias breakdown voltage of the Zener diodes (8VDC each, in-series total 16VDC). C2 integrates the difference between high forward current through the Zeners when the positive phase of the received AC waveform exceeds their forward bias and the low reverse current during the negative phase until they reach their negative Zener threshold. This results in a bias voltage (measurement described in Results) that provides the desired voltage stress across the interleaved electrodes that form C2. Epoxy with dissolved and condensed water form virtual resistors R1 and R2 between the capacitor electrodes shown in the schematic.

A total of 12 comb pattern devices with three different common defects during fabrication process were made to demonstrate sensitivity to failures. 1) Bubble defects were induced intentionally in the epoxy injection step with undegassed epoxy and injection without a vacuum. 2) Finger print oil was introduced after final cleaning by swiping a cotton swab contaminated with finger oil over the surface of the comb pattern before encapsulation. 3) Contamination by a cyanoacrylate adhesive (normally used to mount the PCB and control the terminations of the coil) was applied by hand.

Preliminary work had suggested that epoxy adhesion was adversely affected by using deionized water instead of distilled water in the final rinsing step of the PCB cleaning process before epoxy encapsulation. Two groups of 20 comb pattern devices each were constructed to evaluate the differences using the following cleaning procedures (Table 1) before epoxy encapsulation (as described above): 1) The comb patterns designated “Deion. Clean” were flushed by isopropyl alcohol (IPA) for 30s and brushed if there was visible debris left on the board., then rinsed with deionized water for 30s and dried in the oven for 2 h, and 2) The comb patterns designated “Dist. Clean” were placed in separate clean vials for

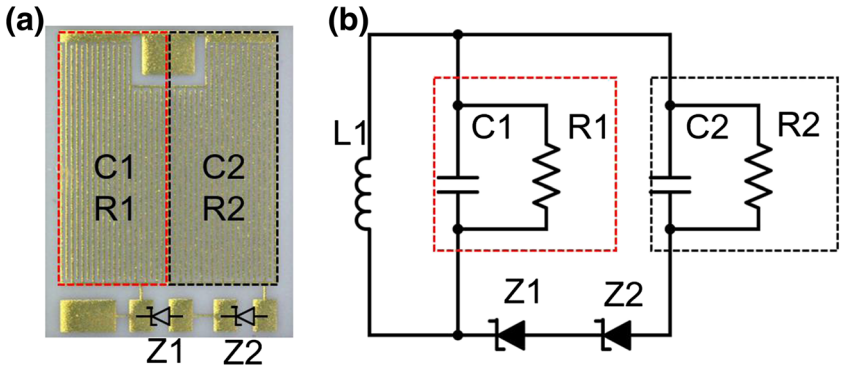

Fig. 2 **a** Comb pattern ceramic PCB board with IDE. **b** Schematic of comb pattern board. C1 and C2 represent the capacitors circled by *red* and *black* dotted lines in the PCB board. R1 and R2 represent virtual resistance in parallel with capacitors. L1 is the winding coil on ferrite. Z1 and Z2 are Zener diodes

Table 1 Comparisons of different cleaning procedure for comb pattern devices in Deion. Clean group, Dist. Clean group and functional microstimulators

	Deion. Clean	Dist. Clean	Microstimulator
Ferrite			detergent (ultrasound, 10 min.) distilled water (rinse, 30s)
Subassembly	IPA (rinse, 30s) IPA (brush) de-ionized water (rinse, 30s) oven dry (2 h)	IPA (ultrasound, 10 min.) distilled water (ultrasound,10 min.) oven dry (2 h)	IPA (ultrasound, 10 min.) distilled water (ultrasound, 10 min.) distilled water (rinse, 30s) oven dry (2 h)

ultrasound cleaning with IPA (10 min.) and distilled water (10 min.), then dried in the oven for 2 h.

2.2 Functional device

After the studies of comb pattern devices, 9 functional microstimulators were fabricated and encapsulated according to the final cleaning procedure as shown in Table 1, which included some further improvements. Before the coil winding procedure, any loose particulates from the machined ferrites were removed by sonicating in detergent for 10 min. (1% detergent in distilled water, Detergent 8, Alconox, NY, USA) and then rinsed with distilled water to flush out residual detergent. The PCB was placed on the ferrite using the same epoxy adhesive as for encapsulation instead of cyanoacrylate. The functional device was cleaned before the wire bonding by the same cleaning procedure as for the final subassembly. The final subassembly was rinsed after ultrasonic cleaning by distilled water to flush out any contaminants from the ultrasonic bath.

2.3 Wireless detection

The bandwidth and resonant frequency of the LC circuit of the comb pattern devices were detected wirelessly by the concentric, orthogonal, inductive coil pair shown in Fig. 3a. The coils were carefully aligned to minimize direct inductive coupling between the transmitter and receiving coils by finding the null orientation at all test frequencies. The function generator (Tektronix AFG3102 Dual Channel Function generator) generated a sinusoidal sweep frequency 16–24 MHz at 10 Vp-p to provide power to the transmitter coil. The device under test was inserted at 45 degrees into the center of both coils. The output voltage of the receiver coil was recorded on the oscilloscope to determine resonant frequency and bandwidth. When the frequency of the transmitted magnetic field equals the resonant frequency of the device under test, it induces a maximal circulating current in the LC circuit. The induced current flow in the coil of the device under test creates its own magnetic field, which is picked up by the receiving coil of the test system. The self-resonant frequency (green trace in Fig. 3b) of a

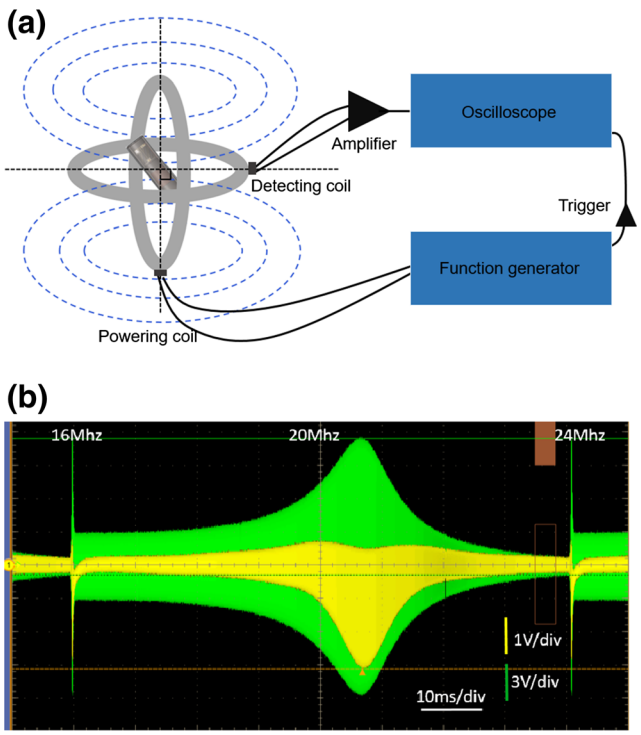

Fig. 3 **a** Two coil wireless query system for resonant frequency and bandwidth detection. The powering coil (2 turns of 18 AWG insulated *copper* wire, 37.5 mm in diameter) and the detecting coil (30 turns 22 AWG insulated *copper* wire, 35 mm in diameter) were placed orthogonally to minimize direct electromagnetic coupling between them. The test article was placed at 45° angle between them so that it coupled to both coils. **b** Oscillogram of self-resonant frequency and bandwidth (*green* trace) as measured in wireless detection, sweeping from 16 to 24 MHz. Generated bias DC voltage (*yellow* trace) on the diodes as measured by needle probes is correlated to device's resonant properties

comb pattern device was measured by the receiving coil as displayed on oscilloscope, which was ~20.7 MHz with ~1 MHz bandwidth before encapsulation. The bias DC voltage (yellow trace in Fig. 3b) was also measured during wireless detection and was found to be correlated with the measured resonant properties of the device under test. Instead of directly probing the comb pattern capacitor, which is the summation of the both the capacitor output and the bias, the bias DC voltage was measured directly using fine needle probes between Zener diodes. The bias DC voltage tended to drop substantially when the self-resonant frequency and/or Q factor of the device was affected by moisture applied on the bare comb pattern board.

2.4 Wireless powering

The comb pattern devices were powered inductively during accelerated life-testing by a custom transmitter coil driven by a class E power amplifier. The external power source produced a 20 MHz continuous electromagnetic field at least 10 A/m strength up to 10 cm distance from the plane of the coil. The design of this RF powering system and methods to measure and optimize power output were similar to those described previously for the microstimulator (Vest et al. 2016). When the devices were around 20 MHz, Q factor at 15, and placed at various distances above the RF transmitter, the measured Zener-regulated bias DC voltage as displayed on oscilloscope was stable at ~11.5 VDC for distances up to 10 cm and tilt angles to 45° from vertical. The bias DC voltage is not regulated at the ideal voltage (16 V) due to component frequency characteristics. During the accelerated life-testing, the resonant frequency and Q factor would drop due to comb pattern capacitance and resistance changes, which decreased the DC bias voltage. The data points in Fig. 4 were acquired by adding different values of capacitors or resistors in parallel with C2 and R2 in the bare comb pattern board, respectively, to shift the resonant frequency or Q factor independently. Fig. 4a plots value of the bias DC voltage as a function of self-resonant frequency when the Q factor was maintained at 15.5 ± 0.4 (mean ± standard deviation). The bias DC voltage dependency on Q factor is shown in Fig. 4b when the self-resonant frequency was maintained at 20.0 ± 0.4 MHz (mean ± standard deviation). By measuring the self-resonance frequency and calculating the Q factor, the bias DC voltage can be conservatively estimated using the fitted curves. For example, if one device had self-resonant frequency at about 19 MHz, the bias voltage would be about 7 V and 4.7 V when Q factor was about 15 and 10, respectively, based on the fitted curve. It is important to note that shifts of this magnitude for resonant frequency and Q were always associated with rapid further shifts that led to device failure as defined below.

2.5 Accelerated life-testing

After initial baseline measurement, all comb pattern devices were positioned vertically inside a saline tank at 50 °C for accelerated life-testing (Fig. 5a) and were removed at regular intervals for wireless detection (Fig. 3a) of their resonant properties. A saline tank was placed over the transmitter coil, and the devices were powered continuously via inductive coupling. Its temperature was monitored by an electromagnetically shielded thermocouple and regulated by a circulating water bath with accuracy of ±1 °C.

If the measured resonant properties of comb pattern devices met the criteria for incipient failure (resonant frequency ≤ 17 MHz), the devices were examined carefully under a microscope to identify possible failure mechanisms. As indicated by the fitted curve in Fig.4, when the resonant frequency was around 17 MHz with Q factor about 7, the voltage stress on the comb pattern dropped below 0.5 V, which would be insufficient to drive most electrolysis reactions. From the preliminary experiments, whenever the self-resonant frequency was lower than 17 MHz or there was no detectable resonant frequency, there were visible gross failures including ionic dissolution, galvanic corrosion and dendrite formation, bridging, and short-circuits between comb pattern traces.

Data was collected for one year in accelerated life-testing. The time to failure of the device was derived from the resonant properties measurement that met failure criteria. An exponential distribution with constant failure rate was assumed for the failure times of two groups of comb pattern devices (Deion. Clean and Dist. Clean groups) (Minnikanti et al. 2014). This was used to extrapolate the reliability of epoxy encapsulation of the microstimulators for 1 year at 37 °C, based on differences in the magnitude and distribution of voltage stress levels between the two types of device. One year of data collection in accelerated life-testing predicts a much longer lifetime than the one year of intermittent use required for the intended clinical application of the neurostimulator.

The acceleration model used in the paper had three combined accelerating factors of temperature, voltage stress and duty cycle. Each individual accelerating factor was assumed to be independent and to contribute to the acceleration multiplicatively (Escobar and Meeker 2006). The accelerated life test was performed at 50 °C, below the glass transition temperature of the epoxy to avoid excessive thermal expansion and glass breakage. The aging factor was determined by an empirical estimation of Arrhenius' Law, for which every 10 °C elevation results in twice acceleration of all chemical reactions (Hukins et al. 2008). The calculated acceleration factor was thus about 2.4 times faster in 50 °C compared to human body environment at

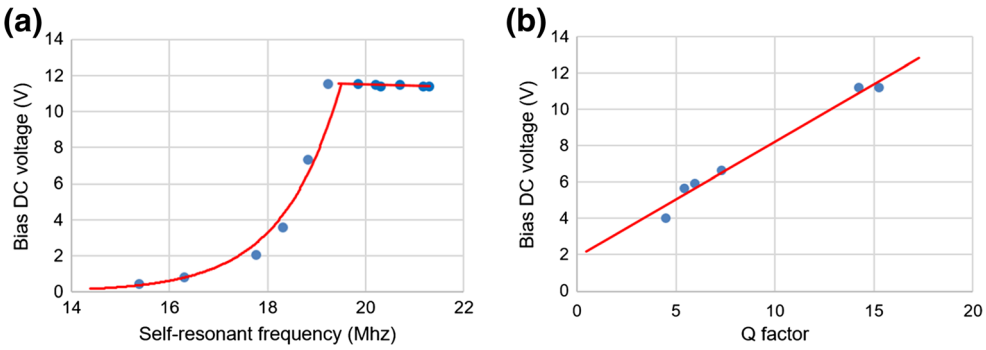

Fig. 4 **a** Measured bias DC voltage as self-resonant frequency changes. **b** Measured bias DC voltage as Q factor changes

37 °C. The inverse power relation was used for non-thermal acceleration due to voltage stress:

$$AF = \left(\frac{E_a}{E_u}\right)^{\beta}$$

where the acceleration factor AF is the ratio between the accelerated voltage stress level and the normal voltage stress level. β =1 assumes that increased voltage stress magnitude has positive, linear acceleration for the device failure. The effects of duty cycle were also estimated from the continuous stress in the accelerated life tester (24 h/d) divided by the maximal daily treatment prescription (2 h/d).

The functional microstimulators were powered in the accelerated life-testing by a separate RF transmitter tuned to the operating frequency of the microstimulator at 6.78 MHz. Rather than placing the devices into saline tank directly as done with the comb pattern devices, each functional microstimulator was loaded into a test vial of saline equipped with Pt-Ir electrodes to capture its output pulses and a light emitting diode (LED) to provide a visual monitor of its functionality (Fig. 5b). The vials were then placed into heated water bath at 50 °C above the RF transmitter. The microstimulator was powered continuously with 20 ms long bursts of RF every 33 ms, generating the maximal stimulus output through the LED of ~3 μC @ 30 pps with peak voltage of 15 V. If and when the LED ceased blinking, the device was removed from the test vial and examined for failure analysis.

3 Results

Measured self-resonant frequency of all comb pattern devices as a function of accelerated life-testing in days is shown in Fig. 6. Details regarding the failure rates for each type of deliberately introduced defect in the comb patterns are shown in Fig. 7. Each trace corresponds to the measurements over time for one device, with color codes to indicate classification according to details of fabrication that were intended to affect reliability. Generally, all devices experienced the same three phases but differed in the rate at which they progressed between phases depending on fabrication classification. In phase 1, self-resonant frequency around 20 MHz dropped within the first couple days of soaking, representing water vapor diffusion into the epoxy encapsulant with dielectric change. In phase 2, if there were no voids or unbounded cavities for water vapor condensation, the measurements were stable with only slight fluctuations that appeared to be related to environmental temperature changes. In phase 3, self-resonant frequency first dropped below 17 MHz, with wide bandwidth and low Q factor due to condensation of moisture, then progressed rapidly towards undetectable resonant frequency, shown as a sharp decline in the plot, representing metal corrosion and

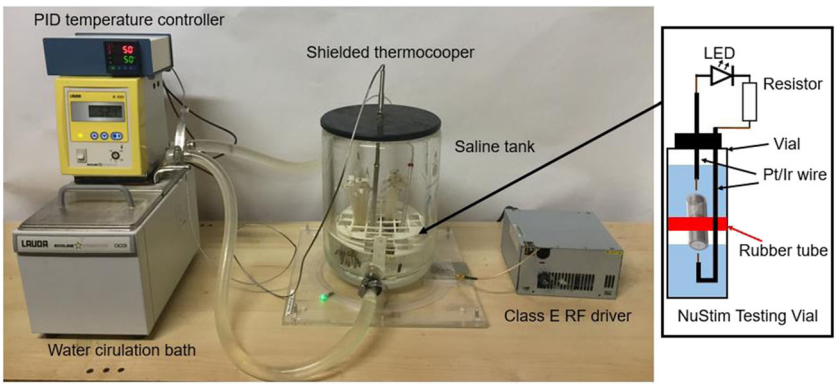

Fig. 5 **a** Accelerated life test system for both comb pattern devices and the microstimulator. **b** Accelerated life-testing vial for the microstimulator to convert stimulation pulses into visible light flashes. The rubber tube acts as an O-ring to force the output stimulation current through the surrounding saline and into the Pt/Ir wire electrodes, which do not touch the output electrodes of the microstimulator

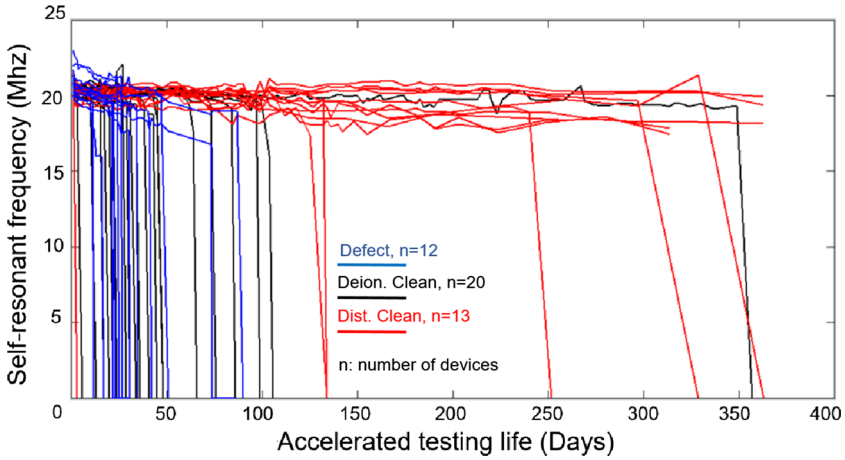

Fig. 6 Self-resonant frequency measurements of all comb pattern devices as a function of number of days in accelerated life-testing

ultimate circuit failure from dendrite growth and shorting between the comb electrodes.

The measured resonant frequency and calculated Q factor of comb pattern devices with different defects over duration of accelerated life testing in days are shown in Fig. 7.

- Fingerprint oil-contaminated devices (red traces in Fig. 7) had slightly higher initial self-resonant frequency than other devices. The epoxy over the fingerprints appeared to have pulled away from the comb pattern electrodes during curing, leaving air-filled spaces between electrodes

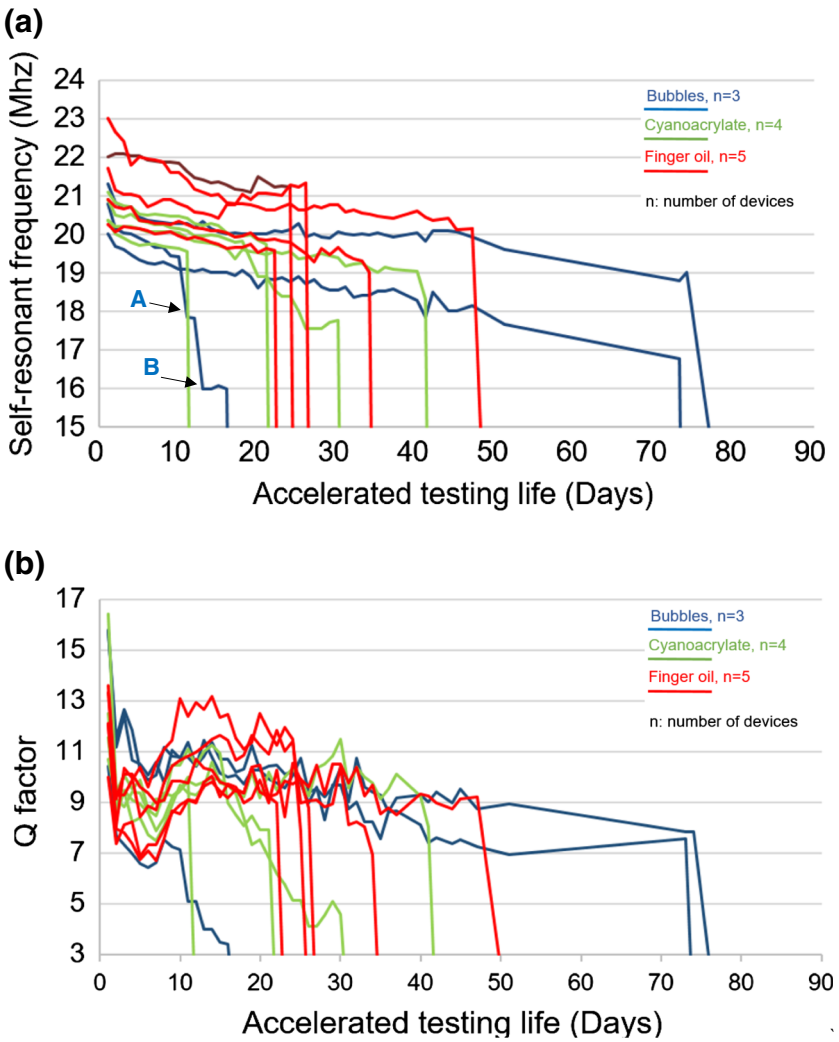

Fig. 7 **a** Self-resosnant frequency measurment of comb pattern devices with defects as function of days in testing. Marker A and B represent day of observation with blistering (Fig. 8d and e) and delamination on gold trace in one device with huge bubble (Fig. 8f). **b** Calculated Q factor as function of days in testing

that had lower dielectric constant than the epoxy. Compared with other devices, the finger print oil contaminated devices usually failed most quickly due to direct water vapor condensation in the void and dendrite formation between electrodes (Fig. 8a).

- Cyanoacrylate-contaminated devices (green traces in Fig. 7) tended to initiate corrosion on the edge of the PCB where the low-viscosity adhesive could seep onto the comb pattern before curing. This was associated with unreliable adhesion, corrosion, dendritic short circuits and undetectable self-resonant frequency (Fig. 8b). The damage could expand even after electrical function ceased (Fig. 8c).
- Bubble-defect devices (blue traces in Fig. 7) usually lasted longer in accelerated life-testing than other devices, except for one device with a huge bubble over the comb pattern that left only a thin layer of epoxy on the electrodes after curing. Water vapor condensation could be found in the bubble after 10 days of soaking (Fig. 8d). Optical microscopy revealed blistering on the gold electrode (Fig. 8e) with progressive delamination (Fig. 8e) that was correlated with resonant frequency measurements (markers A and B on Fig. 7a, respectively).

The percentages of surviving devices in the Deion. Clean and Dist. Clean groups are plotted over time in Fig. 9. The Deion. Clean group had a total of 20 devices subjected to the soaking test, whereas the Dist. Clean group had 13 devices after excluding 7 devices that failed from unrelated manufacturing problems. In the Deion. Clean group, about 50% of devices failed after 30 days and 90% failed after 100 days. In the Dist. Clean group, about 54% (7 of the 13 devices) were still working after more than 365 days in the accelerated life-testing. The surviving comb pattern devices had stable self-resonant frequencies around 19 MHz with Q factor ~ 9, which was estimated to generate 4.2 V voltage stress (see Fig. 5). Corrosion usually started on the gold trace (Fig. 10a) and gradually increased over time (Fig. 10b). Eventually, the epoxy barrier between comb pattern traces broke in at least one location, which led to functional failure (Fig. 10c).

All 9 functional microstimulators were stressed continuously in the accelerated life-testing chamber. The survival rate over time is shown in Fig. 9. Two devices failed after 119 and 155 days; the other 7 devices were still functioning normally after >180 days at 50 °C (equal to ~14 months at 37 °C). The two failed devices were subjected to failure analysis by applying various test signals to their output electrodes. Neither failure was related to epoxy encapsulant failure. One device had no visible corrosion but had no self-resonant frequency; this is most likely caused by a cold solder joint where the copper wire is attached to the ceramic PCB. A procedure to pretin the copper wire before soldering to the PCB was added to alleviate this problem. The other failed device had the characteristic appearance of "purple plague" around one end of the gold bondwire to an aluminum pad on the programmable unijunction transistor in the stimulation circuit (Blish et al. 2007). This is a classic example of interfacial intermetallic compound (IMC) formation when such bonds are poorly made and subjected to high current flow.

4 Discussion

4.1 Interpretation of test data

The measured self-resonant frequency and calculated Q factor of the comb pattern devices are both sensitive indicators of encapsulant performance. They are related to each other, but Q factor provides additional information. In the first several days of testing, capacitance increases as absorbed water vapor increases the dielectric constant of the epoxy encapsulant, which decreases self-resonant frequency (Fig. 7a) and should increase Q factor (Fig. 7b). Instead, the Q factor decreases as the result of significant decrease in resistance based on Eq. 2, which is related to an increase of epoxy conductivity from water vapor dissolved in it (Bierwagen et al. 2003). As more water vapor diffuses through the epoxy, the Q factor then increases, which represents an increase of capacitance due to the expected dielectric change from water vapor with no further change in resistance between traces. When water vapor reaches saturation, the measured Q factor becomes stable, indicating stable capacitance and resistance. If the adhesive bonding is damaged, the resistance between electrodes drops significantly, as indicated by a rapid decrease of Q factor. The comb pattern circuity is not an ideal RLC parallel circuit as shown in Eq. 2. The circuit has additional resistance introduced by the winding coil wire and impedance from the Zener diodes, which complicates the equivalent circuit. Rather than providing quantitative measurements, the circuit allows qualitative evaluation of resistance and capacitance changes from water vapor diffusion and condensation.

One objective of this study is to determine and optimize the long-term reliability of the epoxy encapsulation for a wireless microstimulator. Instead of relying on long-term functional testing of complete devices, a comb pattern is preferable for accelerated identification of failure modes in several ways:

1. It has a large area of high density of closely spaced conductors that are vulnerable to water condensation.

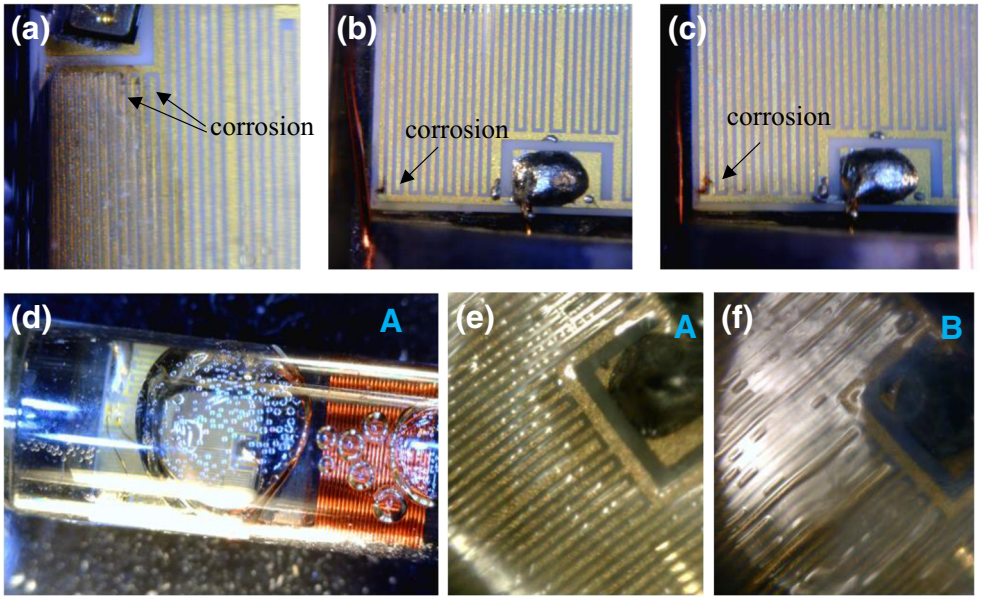

Fig. 8 **a** Typical corrosion on IDE with finger print oil contamination. **b** Typical corrosion on IDE with adhesive contamination. **c** Increased corrosion area over time. **d** and **e** The giant bubble filled with water and blisters forming on the gold traces. Markers A: optical microscopy correlated with measured resonant frequency in Fig. 7a. **f** Further delamination formed along the gold trace. Marker B: optical microscopy was correlated with measured resonant frequency in Fig. 7a

2. High voltage stress can be applied to accelerate incidence of failure without introducing electrical connections that might change failure susceptibility.
3. Water vapor diffusion, condensation and corrosion are detected as changes of capacitance and resistance to provide an early indication of incipient device failure.

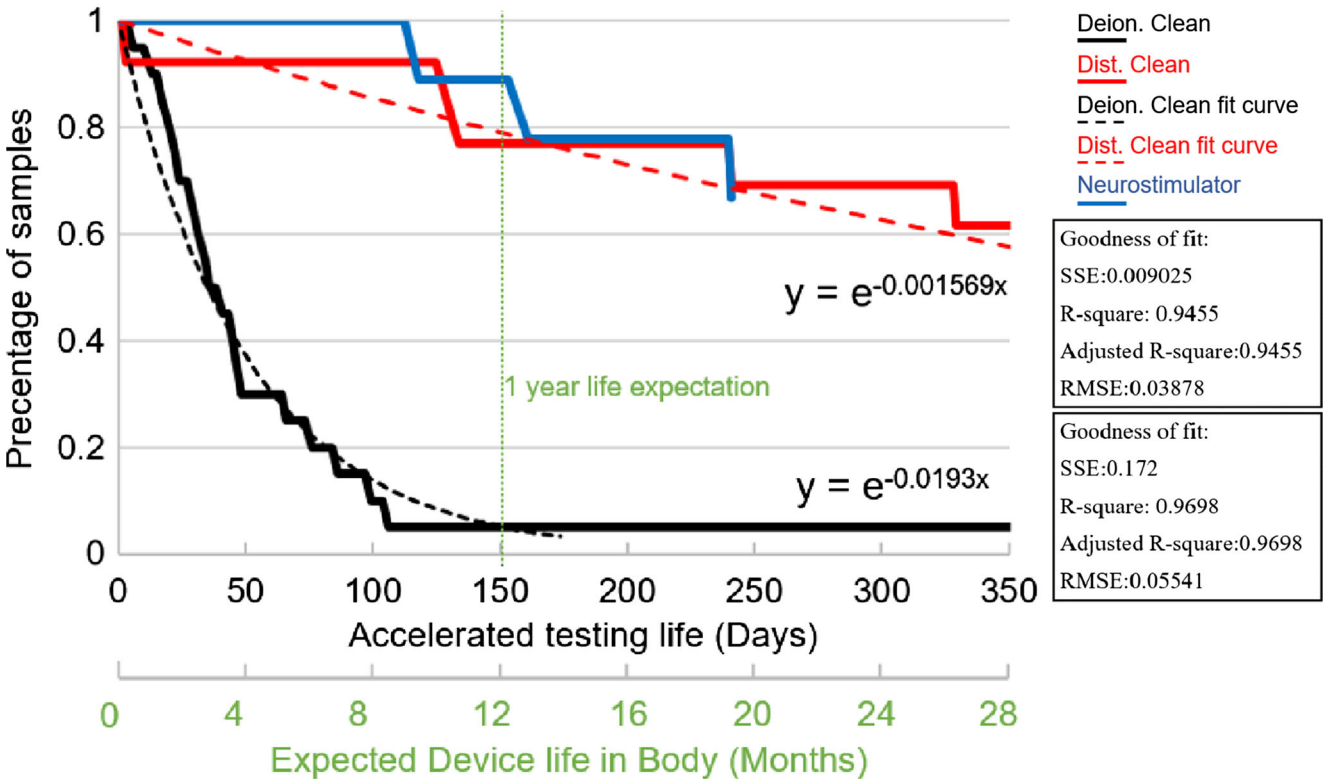

Fig. 9 Number of survived devices in deionized clean group (*Deion. clean*), distilled clean group (*Dist. Clean*) and neurostimulator group as a function of accelerated testing days (normalized to number of devices starting soaking). The x-axis in green represents expected life in months at 37 °C, assuming only Arrhenius temperature acceleration

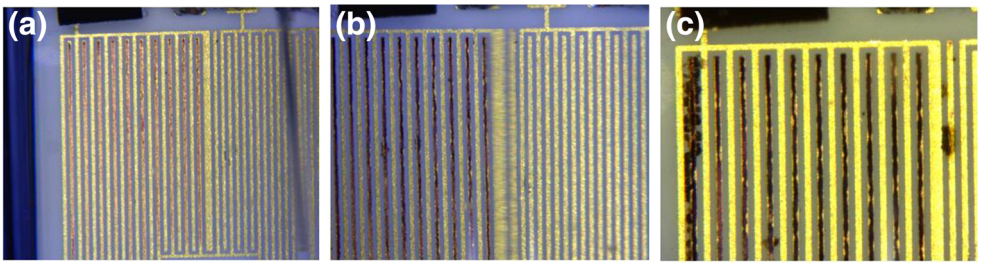

Fig. 10 **a**, **b** and **c** typical corrosion of 100, 220 and 350 days after soaking respectively, visible only on anodally-polarized gold traces

4. These changes can be computed from their effects on self-resonant frequency and bandwidth as measured wirelessly by an external pair of inductive coils.
5. The comb pattern devices can be made using the same materials and processes as the microstimulator, which allows extrapolation and prediction of performance for functional devices.

The last point is especially important, as none of the 9 microstimulators undergoing accelerated life-testing experienced a failure due to encapsulation even after 6 months of testing. Their reliability must be extrapolated from the encapsulation failures of the comb pattern devices, which exhibit large and rapid changes in their normally very high impedance and Q-factor.

4.2 Extrapolation of expected lifetime

The failure rate of the microstimulator encapsulation can be estimated quantitatively by considering the probability of packaging failure in comb pattern devices and correcting for acceleration due to stressors including temperature, voltage stress and duty cycle. Exponential curves were fit to the data of the Deion. Clean and Dist. Clean devices, as shown in Fig. 9 (goodness of fit: R-square about 0.967 and 0.946 respectively). To extrapolate at least 1 year lifetime at 37 °C, the device should last 152 days at 50 °C, based on 2.4 aging factor due to temperature. The 1 year calculated reliability is 5.3% and 78.8% for Deion. Clean and Dist. Clean respectively. The reliability of 78.8% in one year can be interpreted as probability of success of a random device in the Dist. Clean group to last at least for 1 year, which can be expressed as the following equation,

$$P_{\text{sucsess rate}} = 78.8\% = e^{-0.001569*152} = \textit{Re}\text{liability in } \textit{one} \text{ year} \quad (4)$$

This probability assumes that failures only occur on the half of the comb pattern device that was subjected to voltage stress from the DC bias, as was observed. This half comb pattern has total length of parallel electrodes about $l = 40mm$. If an occurrence of failure is linearly distributed on this 40 mm electrode plate with a constant probability, and if the occurrence of each failure point is independent, the probability of success of the comb pattern can be assumed as the product of success probabilities of all forty units of electrodes with length $l = 1\ mm$, which can be described as

$$P_{\text{success rates}} = \left(P_{s(\text{unit}=1mm)}\right)^{40} \quad (5)$$

The calculated success probability of a unit $P_{s(unit=1\ mm)}$ is equal to 99.41%, which means only 0.59% chance that a failure will occur on the 1 mm long parallel plate electrodes at the voltage stress E_{comb}. The traces subjected to high voltage stress E_{NuStim} in the microstimulator are about 1 mm in length with measured distance between traces about 150 μm. The probability to fail on the unit length at 1 mm on comb pattern device is assumed to be same in the microstimulator after correcting for the different voltage stress (see below Eq. 7). The voltage aging factor $AF_{voltage}$ between the microstimulators and comb pattern devices is determined by the inverse power relationship. In the accelerated life-testing, the microstimulator is powered 24/7 at its maximal rated output. In actual practice, the microstimulator will be only used by patients for no more than 2 h per day in the targeted treatment of stress urinary incontinence. Because the increase of use rate is assumed to accelerate the device failure linearly (Xie et al. 2015), the aging factor of use rate $AF_{use\ rate}$ is increased by a factor of 12 in continuous use as shown in Eq. 8 (This factor will be even larger for likely use conditions at lower frequencies and/or lower pulse strengths, which reduce the duty cycle of the RF bursts powering each output pulse of the implant). Overall, the following derived equation can be used to provide quantitative estimation of encapsulant failure fate of the microstimulator,

$$P_{f(\text{NuStim})} = P_{f(\text{unit}=1mm)} \cdot \frac{1}{AF_{\text{voltage}}} \cdot \frac{1}{AF_{use\ \text{rate}}} \quad (6)$$

$$\text{Where, } AF_{\text{voltage}} = \left(\frac{E_{\text{comb}}}{E_{\text{NuStim}}}\right)^{\beta} = \left(\frac{\frac{V_c}{d_c}}{\frac{V_N}{d_N}}\right)^{\beta} \quad (7)$$

$$\text{Where, } AF_{\text{userate}} = \frac{24\ hrs}{2\ hrs} \quad (8)$$

In Eq.6, $P_{f(NuStim)}$ is the probability of the microstimulator epoxy encapsulant failure after one year of maximal intended use in the human body. $P_{f(unit=1\ mm)}$ is the probability of

failure of the comb pattern, which is 0.59%. The aging factor of voltage $AF_{voltage}$ is 1.64, where voltage stress E_{comb} = 168 *V/mm* with V_c = 4.2 *V* and d_c = 25 μm, and voltage stress E_{NuStim} = 100 *V/mm* with V_c = 15 *V* and d_c = 150 μm, with assumption of β = 1 indicating a linear effect of voltage stress.

The quantitative estimation of the microstimulator failure rate at one year $P_{f(NuStim)}$ is about 0.03% based on consideration of aging factors from temperature, voltage stress and use rate. This estimated rate is surprisingly low but further supported by the observed result in the microstimulator accelerated life-testing, which had no devices failed due to encapsulation after 180 days testing at elevated temperature and maximal output. All devices (excluding the two that failed for other reasons) have functioned for the equivalent of >1 year at 37 °C (the original design goal for the clinical application) despite continuous powering. This conclusion must be tempered by the relatively small number of devices tested to date, which results in a relatively large statistical uncertainty about actual reliability. The accelerated life-test methods described herein now need to be applied systematically to larger samples of devices. According to parametric binomial statistics, 36 comb pattern device samples with 4 failures occurring over 152 days in accelerated life-testing would demonstrate the claimed reliability at a 90% confidence level (Guo et al. 2013). The much higher reliability extrapolated for the microstimulators would require a much larger sample and/or a much longer test period to confirm empirically. Conversely, failures occurring more frequently would suggest failure modes different from those related to the epoxy encapsulation in the comb pattern devices.

Non-hermetic encapsulation relies on adhesive bonding to the component surfaces that is maintained by electrostatic attraction and mechanical interlocking (Yacobi et al. 2002). The cleaning procedure is a critical step for encapsulation performance because even a monolayer of a surface contaminant can prevent the necessary bonds from forming. The major contaminant residue left on a populated circuit board is flux in the solder paste. It is formulated from many ionic and organic compounds that include reactive species. The soldering problem can be managed by using water soluble solder paste. The deionized water was not as effective as distilled water to clean the subassembly. Deionization removes ions such as sodium and chloride but may leave or even introduce non-ionic contaminants. Deionized water is typically shipped and stored in plastic bottles, from which oligomers, catalysts, and plasticizers may leech. Water distilled and stored in glass bottles should be used for final rinses to prevent contaminants from coating surfaces after the water evaporates away. The fully cured epoxy Epotek 302-3 M has high chemical stability, strong dielectric properties, low water uptake and slow diffusion rate; it was found to be a reliable encapsulant (Birkelund et al. 2011). Low permeability itself cannot prevent water vapor diffusion throughout a device as small as the microstimulator, but it tends to be associated with low water absorption; such absorption and swelling can produce mechanical stresses that may disrupt chemical adhesion, leaving voids for water condensation. Strong adhesion between encapsulant and active circuitry can reliably prevent water vapor condensation and corrosion for many years (Donaldson 1991). Although the epoxy thermal expansion would induce extra pressure, thereby improving adhesion and decreasing the likelihood of delamination, it is negligible in this study due to the small cross-sectional area of the epoxy above the PCB and the low thermal expansion coefficient.

Although the comb pattern device has been made to mimic the fabrication process of the functional wireless microstimulator, there are still several differences that may affect the encapsulation performance in various ways. First, the microstimulator has more discrete components and complicated structure than the comb pattern device, which has only two Zener diodes on the PCB located away from the sensitive interdigitated electrodes. Compared to the unbroken flat surface of the comb pattern, the microstimulator might be subjected to residual stress due to non-uniform shrinkage and shear forces from epoxy curing, which could introduce potential voids for water vapor condensation. Although hybrid discrete electronic components are generally not vulnerable to water vapor, these components and their solder joints are susceptible to liquid water that might condense in a void between components and circuit board or a cavity within a component. The cleaning procedure is sufficient to get rid of contamination on the board when components are placed and soldered properly. The controlled low rate of epoxy infiltration and curing under pressure can help epoxy penetration into cavities and compress any residual bubbles to provide a defect-free encapsulation (Loos and Springer 1983). Second, wire-bonding in microelectronic circuits is another vulnerability with its own failure modes, which were not present in the comb pattern devices. The thermosonic gold wire-bonding to aluminum pads in the microstimulator inevitably forms intermetallic compounds at the junction that tend to have poor electrical conductivity, the source of the purple-plague failure of one device. Wire-bond quality is controlled by proper cleaning procedure before bonding and the settings of the wire-bonding machine. Our cleaning procedure used ultrasound with solvents to clean the pad surface, resulting in mechanically acceptable wire-bonds with a breaking force of 7 to 12 g. The thickness and resistance of the intermetallic compound at the gold-aluminum junction needs to be minimized by providing an appropriate substrate temperature during bonding (Breach and Wulff 2004, Xu et al. 2010).

5 Conclusion

We have evaluated the functional long-term reliability of miniature, implantable, wireless electronic devices that rely on

non-hermetic, epoxy encapsulants. The lifetime was measured by an encapsulated comb pattern with high density of interdigitated electrodes that was used to detect incipient failures. The capacitance of the comb pattern forms a resonant circuit with the inductor by which the implant receives power. Any moisture affects both the resonant frequency and the Q-factor of the resonance, which was detected wirelessly by its effects on the coupling between two orthogonal RF coils placed around the device. Inductive coupling of an RF magnetic field was used in the accelerated life-testing to provide DC bias. Strong adhesive bonding between epoxy and electronic circuity proved to be necessary for package reliability; this can be achieved by proper cleaning and encapsulation procedures. Comb pattern devices were estimated to have 78.8% reliability for one year, which extrapolated to 1 year reliability of 99.97% for the neuromuscular stimulator after accounting for various stressors in the accelerated life-test. This is consistent with the results from accelerated life-testing of a small sample of the microstimulators, in which there were no encapsulant failures even beyond 6 months of continuous output at elevated temperature.

Acknowledgements The authors would like to thank engineers Ray Peck, Sisi Shi, and Longpeng Jiao for help in design and manufacturing. The project is funded by General Stim Inc.

References

G. Bierwagen, D. Tallman, J. Li, L. He, C. Jeffcoate, EIS studies of coated metals in accelerated exposure. Prog Org Coat **46**(2), 149–158 (2003)

K. Birkelund, L. Nørgaard, E.V. Thomsen, Enhanced polymeric encapsulation for MEMS based multi sensors for fisheries research. Sensors Actuators A Phys. **170**(1), 196–201 (2011)

R.C. Blish, S. Li, H. Kinoshita, S. Morgan, A.F. Myers, Gold–aluminum intermetallic formation kinetics. IEEE Trans. Device Mater. Reliab. **7**(1), 51–63 (2007)

C. Breach, F. Wulff, New observations on intermetallic compound formation in gold ball bonds: General growth patterns and identification of two forms of au 4 al. Microelectron. Reliab. **44**(6), 973–981 (2004)

J. G. Chubbuck, Intracranial pressure monitor, Google Patents (1977)

P. Donaldson, Aspects of silicone rubber as an encapsulant for neurological prostheses. Med. Biol. Eng. Comput. **29**(1), 34–39 (1991)

Escobar, L. A. and W. Q. Meeker. "A review of accelerated test models." Statistical science: 552–577 (2006)

H. Gensler, R. Sheybani, P.-Y. Li, R.L. Mann, E. Meng, An implantable MEMS micropump system for drug delivery in small animals. Biomed. Microdevices **14**(3), 483–496 (2012)

H. Guo, E. Pohl, A. Gerokostopoulos, Determining the right sample size for your test: theory and application. 2013 Annual Reliability and Maintainability Symposium, Available from http://www.reliasoft.com/pubs/2013_RAMS_determining_right_sample_size.pdf. Accessed on 5 June 2014 (2013)

C. Hassler, T. Boretius, T. Stieglitz, Polymers for neural implants. J. Polym. Sci. B Polym. Phys. **49**(1), 18–33 (2011)

D. Hukins, A. Mahomed, S. Kukureka, Accelerated aging for testing polymeric biomaterials and medical devices. Med. Eng. Phys. **30**(10), 1270–1274 (2008)

S. Kim, R. Bhandari, M. Klein, S. Negi, L. Rieth, P. Tathireddy, M. Toepper, H. Oppermann, F. Solzbacher, Integrated wireless neural interface based on the Utah electrode array. Biomed. Microdevices **11**(2), 453–466 (2009)

A. Koulaouzidis, D.K. Iakovidis, A. Karargyris, E. Rondonotti, Wireless endoscopy in 2020: Will it still be a capsule? World J. Gastroenterol. **21**(17), 5119–5130 (2015)

G.E. Loeb, R.A. Peck, W.H. Moore, K. Hood, BION™ system for distributed neural prosthetic interfaces. Med. Eng. Phys. **23**(1), 9–18 (2001)

A.C. Loos, G.S. Springer, Curing of epoxy matrix composites. J. Compos. Mater. **17**(2), 135–169 (1983)

S. Minnikanti, G. Diao, J.J. Pancrazio, X. Xie, L. Rieth, F. Solzbacher, N. Peixoto, Lifetime assessment of atomic-layer-deposited Al2O3–Parylene C bilayer coating for neural interfaces using accelerated age testing and electrochemical characterization. Acta Biomater. **10**(2), 960–967 (2014)

W. Nelson, Accelerated life testing-step-stress models and data analyses. IEEE Trans. Reliab. **29**(2), 103–108 (1980)

K.G. Ong, C.A. Grimes, A resonant printed-circuit sensor for remote query monitoring of environmental parameters. Smart Mater. Struct. **9**(4), 421 (2000)

T. Stieglitz, Manufacturing, assembling and packaging of miniaturized neural implants. Microsyst. Technol. **16**(5), 723–734 (2010)

A. Vanhoestenberghe, N. Donaldson, Corrosion of silicon integrated circuits and lifetime predictions in implantable electronic devices. J. Neural Eng. **10**(3), 031002 (2013)

A.N. Vest, L. Zhou, X. Huang, V. Norekyan, Y. Bar-Cohen, R.H. Chmait, G.E. Loeb, Design and testing of a transcutaneous RF recharging system for a fetal Micropacemaker. IEEE Trans Biomed Circuits Syst **11**(2), 336–346 (2016)

P. Wang, S. Lachhman, D. Sun, S. Majerus, M.S. Damaser, C.A. Zorman, P.-L. Feng, W. Ko, *Non-hermetic micropackage for chronic implantable systems* (International Symposium on Microelectronics, International Microelectronics Assembly and Packaging Society, 2013)

X. Xie, L. Rieth, R. Caldwell, S. Negi, R. Bhandari, R. Sharma, P. Tathireddy, F. Solzbacher, Effect of bias voltage and temperature on lifetime of wireless neural interfaces with Al2O3 and parylene bilayer encapsulation. Biomed. Microdevices **17**(1), 1–8 (2015)

H. Xu, C. Liu, V.V. Silberschmidt, S. Pramana, T.J. White, Z. Chen, M. Sivakumar, V. Acoff, A micromechanism study of thermosonic gold wire bonding on aluminum pad. J. Appl. Phys. **108**(11), 113517 (2010)

X. Huang, K. Zheng, S. Kohan, M. Denprasert, L. Liao, G.E. Loeb, *Neurostimulation strategy for stress urinary incontinence* (Transactions on Neural Systems and Rehabilitation Engineering, IEEE, 2017)

B. Yacobi, S. Martin, K. Davis, A. Hudson, M. Hubert, Adhesive bonding in microelectronics and photonics. J. Appl. Phys. **91**(10), 6227–6262 (2002)

L. Zhou, A.N. Vest, R.A. Peck, J.P. Sredl, X. Huang, Y. Bar-Cohen, M.J. Silka, J.D. Pruetz, R.H. Chmait, G.E. Loeb, Minimally invasive implantable fetal micropacemaker: Mechanical testing and technical refinements. Med Biol Eng Comput **54**(12), 1819–1830 (2016)